Optical Properties of an Ionic-Type Phononic Crystal

Yan-qing Lu, *et al.*

Science **284**, 1822 (1999);
DOI: 10.1126/science.284.5421.1822

Science (print ISSN 0036-8075; online ISSN 1095-9203) is published weekly, except the last week in December, by the American Association for the Advancement of Science, 1200 New York Avenue NW, Washington, DC 20005.

Optical Properties of an Ionic-Type Phononic Crystal

Yan-qing Lu,[1] Yong-yuan Zhu,[1] Yan-feng Chen,[1] Shi-ning Zhu,[1] Nai-ben Ming,[1]* Yi-Jun Feng[2]

An ionic-type phononic crystal composed of two ferroelectric media with opposite spontaneous polarization aligned periodically in a superlattice structure was studied theoretically and experimentally. The coupling between vibrations of the superlattice and the electromagnetic waves results in various long-wavelength optical properties, such as microwave absorption, dielectric abnormality, and polariton excitation, that exist originally in ionic crystals. The results show that this artificial crystal structure can be used to simulate the microscopic physical processes in real crystals.

Study of the periodic medium has long been a topic of interest. In a crystal, the periodic potential causes the energy structure of electrons to form a band structure with only those electrons in pass bands that are capable of moving freely. In artificial composites such as superlattices, the periodic modulation of the related physical parameters may also result in band structure and novel properties. Associated with the variation of dielectric constants is the photonic crystal (*1*), which is important for applications such as suppressing spontaneous emission, manipulating light in a specific path, and creating novel laser geometries (*1, 2*). The modulation of nonlinear optical coefficients results in a quasi–phase-matched frequency conversion that is more efficient than that with a birefringence phase-matching method (*3, 4*). Recently, interest in phononic crystal, a periodic elastic composite, has grown (*5–7*). Attention has been given to phenomena such as Anderson localization (*8*) and possible applications such as acoustic filters and new transducers (*5–7*). The structure modulation may be extended to quasi-periodic (*9*) or aperiodic structures, and the modulation parameters may be more complicated. For example, objects such as the ferroelectric domain or piezoelectric coefficient may be modulated. Even two or more parameters may be modulated together, which could result in some coupling effects.

In a real crystal, various couplings exist between the motions of electrons, photons, and phonons. For example, infrared absorption and polariton excitation results from the coupling between lattice vibrations and electromagnetic (EM) waves in an ionic crystal. If the ferroelectric domain or piezoelectric coefficient is modulated in a phononic crystal, the interaction between the superlattice vibrations and EM wave may be established. Similar effects can be expected in such an artificial medium. This kind of phononic crystal is termed an ionic-type phononic crystal (ITPC).

To calculate the dispersion relation of phononic crystals, several effective theories have been proposed (*6, 10, 11*). For a one-dimensional (1D) phononic crystal, a simple model can be suggested, which is similar to the 1D atom chain model in real crystals. As we know, there are infinite degrees of freedom (DOF) of vibration of a real object. However, the fundamental vibration may be characterized as that of an equivalent single or finite DOF system, which is the basis of the so-called normal mode method or lumped-parameter method for studying the vibration characteristics of a continuous system (*12*). According to this idea, the fundamental thickness vibration of a free thin plate can be equivalent to the vibration of a spring with two identical mass dots at the terminals. The equivalent mass m^* and the equivalent force constant β^* are determined as $m^* = \rho A l/2$ and $\beta^* = (\pi^2 v^2/4l)\rho A$ for keeping the fundamental frequency unchanged, where ρ, A, l, and v are the density, cross-section area, thickness, and sound velocity of the plate, respectively. Thus, a periodic combination of two kinds of thin plates, A and B, can be viewed as a diatomic chain. The mass of each "atom" is $m = m^*_A + m^*_B$, and the force constants are β^*_A and β^*_B, respectively. The sites of the atoms are at the joints of adjacent plates, which means that the mass is viewed as being concentrated at the boundary of neighboring domains. From the wavelike behavior and traveling wave solution of the motion equation, the dispersion relation of a 1D phononic crystal is obtained with

$$\omega_{\pm}^2 = \frac{\beta^*_A + \beta^*_B}{m} \pm \frac{1}{m}\sqrt{\beta^{*2}_A + \beta^{*2}_B + 2\beta^*_A\beta^*_B\cos[k(l_A + l_B)]} \quad (1)$$

where ω_+ and ω_- correspond to the optic branch and acoustic branch, respectively, and k is the wave vector. At the edge of the Brillouin zone [$k = \pi/(l_A + l_B)$], a phononic band gap appears, which is the same as the result deduced by other methods.

Here, we consider a 1D phononic crystal combined with two ferroelectric media with their spontaneous polarization aligned in opposite directions (Fig. 1A). The boundaries of neighboring domains are charged differently; thus, the domain boundary can be viewed not only as the concentration of mass but also as the charge center. This phononic crystal can be viewed as a 1D diatom chain with positive and negative "ions" connected periodically, similar to a real ionic crystal, therefore forming an ITPC.

In an ITPC, the two kinds of ions constitute dipoles whose relative motion can be influenced by an EM field, especially that of a microwave. Because the wave vector of a microwave is much smaller than the width of the Brillouin zone, the microwave interacts only with optic branch phonons at the center of the Brillouin zone ($k \approx 0$), giving rise to some typical long wavelength optical properties. Similar to an ordinary ionic crystal, the fundamental equations of the coupled motion can be written as

$$\begin{cases} \ddot{\mathbf{W}} = b_{11}\mathbf{W} + b_{12}\mathbf{E} & (2) \\ \mathbf{P} = b_{21}\mathbf{W} + b_{22}\mathbf{E} & (3) \end{cases}$$

where $\ddot{\mathbf{W}}$ is the second derivative of $\mathbf{W}$ with respect to time; $\mathbf{W}$ represents the relative motion of positive and negative ions; $\mathbf{E}$ is the electric field of the microwave; $\mathbf{P}$ is the polarization induced by the electric field and relative motion of different ions; and b_{11}, b_{12}, b_{21}, and b_{22} are undetermined parameters. In a real crystal, the counterpart equations are those first proposed (*13*) when the

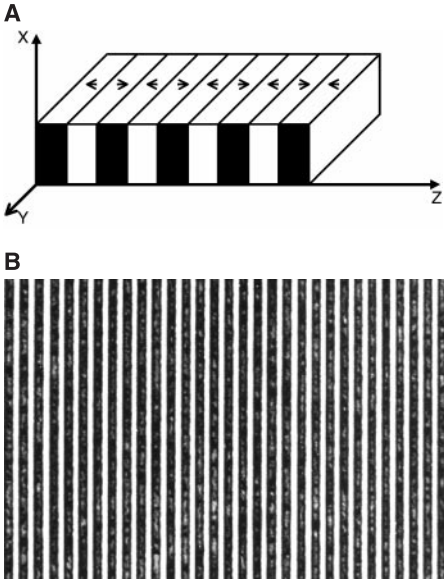

Fig. 1. (**A**) Schematic of an ITPC consisting of two kinds of ferroelectric media. The arrows represent the orientation of the spontaneous polarization. (**B**) Optical microscope photograph showing the periodic ferroelectric domain structure of the etched Y-cut face in an ITPC. The modulation period is 7.2 μm.

[1]National Laboratory of Solid State Microstructures, [2]Department of Electronic Science and Engineering, Nanjing University, Nanjing 210093, People's Republic of China.

*To whom correspondence should be addressed.

coupled motion of lattice and EM waves was studied. In an ITPC, the relative motion is caused by the piezoelectric effect, which implies that vibrations of ITPCs can interact with EM waves even if the constituents of ITPCs are piezoelectric and not ferroelectric.

In piezoelectric materials, the fundamental equations are piezoelectric equations

$$\begin{cases} \sigma = cS - e\mathbf{E} & (4) \\ \mathbf{P} = eS + \varepsilon_0(\varepsilon - 1)\mathbf{E} & (5) \end{cases}$$

where S is strain, σ is stress, ε is the original dielectric constant, c is the elastic constant, and e is the piezoelectric coefficient. These equations reflect the coupling of the elastic wave and the electric field. Naturally, one would ask if there is any relation between the equations in (*13*) and the piezoelectric equations. The simplest case in which the ITPC is composed of two domains with the same thickness and elastic properties was chosen. The only difference between the neighboring domains is that their spontaneous polarizations are aligned oppositely. Because the piezoelectric coefficient is a third-order tensor, it changes its sign from the positive domains to the negative domains. The motion of domain boundaries with positive and negative charges is defined as $\mathbf{U}_+$ and $\mathbf{U}_-$, respectively. Under the condition of long-wavelength approximation, the motion of each primitive cell can be viewed as identical. Thus, using Newton's motion law and treating the ITPC as a 1D chain with discrete equivalent mass dots at domain boundaries, we obtain the equations of the relative motion of these mass dots

$$\begin{cases} \ddot{\mathbf{W}} = -\dfrac{\pi^2 v^2}{l^2}\mathbf{W} + \dfrac{2e}{\sqrt{\rho}l}\mathbf{E} & (6) \\ \mathbf{P} = \dfrac{2e}{\sqrt{\rho}l}\mathbf{W} + \varepsilon_0(\varepsilon - 1)\mathbf{E} & (7) \end{cases}$$

where $\mathbf{W} = (\rho/l)^{1/2}/2(\mathbf{U}_+ - \mathbf{U}_-)$ and l is the domain thickness.

Comparing Eqs. 6 and 7 with Eqs. 2 and 3, one finds that they have the same format, which means that the equations in (*13*) and the piezoelectric equations are equivalent. Thus, parameters in Eqs. 2 and 3 are acquired as $b_{11} = -\pi^2 v^2/l^2$, $b_{12} = b_{21} = 2e/\rho^{1/2}l$, and $b_{22} = \varepsilon_0(\varepsilon - 1)$. According to the procedure for studying the long-wavelength optical properties of ionic crystal, the following results can be obtained from Eqs. 6 and 7 and Maxwell's equations.

The eigenfrequency of the transverse vibration without the coupling of external electric field is $\omega_{T0} = \omega_0 = (-b_{11})^{1/2}$, whereas the eigenfrequency of the longitudinal wave is $\omega_{L0} = [-b_{11} + b_{12}^2/(\varepsilon_0 + b_{22})]^{1/2}$; ω_{L0} is larger than ω_{T0}. Their ratio is described by the Lyddane-Sachs-Teller (LST) relation

$$\frac{\omega_{L0}}{\omega_{T0}} = \left[\frac{\varepsilon(0)}{\varepsilon(\infty)}\right]^{1/2} \quad (8)$$

where $\varepsilon(0)$ is the dielectric constant at low frequency and $\varepsilon(\infty)$ represents the dielectric response that occurs at frequencies much higher than the eigenfrequency of ITPCs. They can be determined as $\varepsilon(\infty) = \varepsilon$ and $\varepsilon(0) = -b_{12}^2/b_{11}\varepsilon_0 + \varepsilon$.

When an EM wave propagates in an ITPC, the electric field stimulates a long-wavelength optic branch vibration in the ITPC and then causes an intensive attenuation of the electric energy at a specific frequency. The absorption power is related to the imaginary part of the dielectric constant, which can be deduced from Eqs. 6 and 7. By including a damping term $-\gamma\dot{\mathbf{W}}$ in the right side of Eq. 6, we get

$$\varepsilon''(\omega) = \frac{b_{12}^2\omega\gamma}{\varepsilon_0[(\omega^2 + b_{11})^2 + \omega^2\gamma^2]} \quad (9)$$

From Eq. 9, the absorption peak locates at $\omega = (-b_{11})^{1/2} = \omega_{T0}$ with the width of γ. This absorption in ITPCs is equivalent to the infrared absorption in ionic crystals, but the frequency determined by the period of ITPC is normally in the microwave band.

Near the eigenfrequency of ITPC, the EM wave interacts with the mechanical vibration strongly; thus, the transverse mode is neither a pure photon mode nor a pure optic branch phonon mode in this narrow range of k values. It is called a polariton mode, a coupling mode of photons and optic branch phonons. This was first predicted in real ionic crystals (*13*) and confirmed experimentally in 1964 (*14*). Our results show that the polariton also exists in ITPCs.

We have calculated the polariton dispersion curve of an ITPC based on periodically poled $LiNbO_3$ (PPLN) with the period of 7.2 μm by taking $\gamma = 0$, which makes ε and therefore k real (Fig. 2). The eigenfrequencies of the transverse wave and longitudinal wave are $f_{T0} = \omega_{T0}/2\pi = 500$ MHz and $f_{L0} = \omega_{L0}/2\pi = 532$ MHz, respectively (*15*). There is a band gap in which the dielectric constant is negative. The corresponding refractive index becomes imaginary. The incident radiation with these frequencies will be reflected. However, this gap does not originate from the interference of EM waves due to the periodic structure but, rather, originates from the interaction of the photon and the transverse optics phonon.

For verification of the predictions above, an ITPC based on PPLN with the period of 7.2 μm was fabricated by the growth striation method (*4*). Its microscopic domain structure was revealed after hydrogen fluoride etching (Fig. 1B). A Y-cut 1.7-mm-thick sample with a pair of Ag electrodes (2.0 mm by 2.0 mm) deposited on each surface was selected for the experiments.

With an HP8510C network analyzer, the reflection coefficient (S_{11}) of the ITPC was measured to simulate the situation in which a microwave beam propagates in the sample. Under this condition, the electric field was applied on the sample simultaneously ($k = 0$), which coincides with the long-wavelength approximation used above. As the microwave wavelength is much larger than the dimension of the electrodes, this assumption is reasonable. The re-

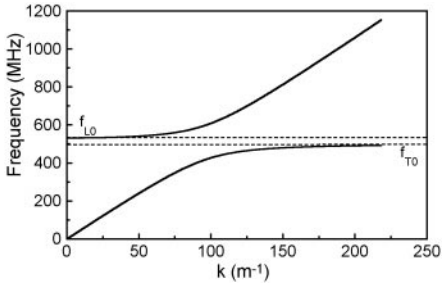

Fig. 2. The calculated polariton dispersion curve of an ITPC with the period of 7.2 μm without consideration of damping. There is a frequency gap between f_{LO} and f_{TO} where no EM waves are permitted to propagate in the sample.

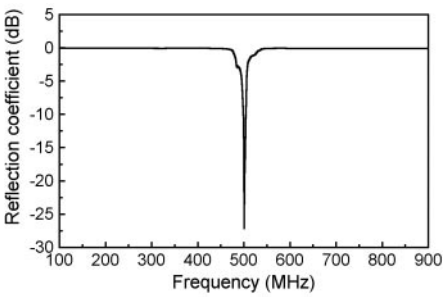

Fig. 3. The measured reflection coefficient of an ITPC in the microwave band. The minimum of the reflection coefficient indicates that there is a strong microwave absorption peak at 502 MHz.

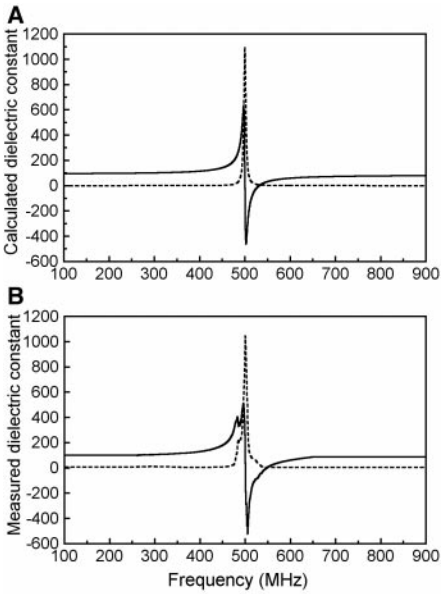

Fig. 4. The dielectric constant curves of an ITPC. The solid lines represent the real part, and the dashed lines represent the imaginary part. (**A**) The calculated result obtained by choosing proper damping ($\gamma = 0.01\omega_{T0}$). (**B**) The measured dielectric constant.

flection coefficient as a function of frequency (Fig. 3) shows that there is an absorption peak ($S_{11} = -26$ dB) at 502 MHz, which is very close to the theoretical value $f = f_{T0} = 500$ MHz.

The dielectric constant was measured by an impedance-analyzing method in order to demonstrate the polariton excitation in ITPC. The results (Fig. 4) are compared with the theoretical results by choosing the proper damping term ($\gamma = 0.01\omega_{T0}$). The dielectric constant changed near ω_{T0}, caused by the superlattice in ITPC. The dielectric spectrum in this band has the same curve shape as the far-infrared dielectric constant of an ionic crystal caused by lattice vibration, showing that they have a similar origin. Much information on the ITPC can be obtained from the dielectric constant curve. The measured f_{T0}, f_{L0}, $\varepsilon(0)$, and $\varepsilon(\infty)$ values are 502 MHz, 547 MHz, 99.88, and 88.02, respectively. They all agree well to the theoretical predictions. The LST relation was also proved, which is $\omega_{L0}/\omega_{T0} = 1.09$, only a slight deviation from the value of $[\varepsilon(0)/\varepsilon(\infty)]^{1/2}$ (1.07). The absorption peak in Fig. 3 is at the same position of the peak of the $\varepsilon''(\omega)$, just as predicted. There is a gap between ω_{T0} and ω_{L0} where $\varepsilon < 0$ and incident EM waves will be strongly reflected. The phenomena above show that there is a polariton mode in ITPC.

From the similarity between the real ionic crystal and the ITPC, other long-wavelength optical properties (such as Raman and Brillouin scattering) might also be expected in an ITPC. The only difference is that they occur in different frequencies. For example, Raman scattering appears in the terahertz region for a real ionic crystal, whereas it might appear in the gigahertz region for an ITPC. Study on these effects is of fundamental interest in physics.

References and Notes

1. E. Yablonovitch, *Phys. Rev. Lett.* **58**, 2059 (1987).
2. _____, T. J. Gmitter, K. M. Leung, *ibid.* **67**, 2295 (1991); A. Mekis *et al.*, *ibid.* **77**, 3787 (1996); Y. S. Chan *et al.*, *ibid.* **80**, 956 (1998); M. M. Sigalas *et al.*, *Microwave Opt. Technol. Lett.* **15**, 153 (1997); J. S. Foresi *et al.*, *Nature* **390**, 143 (1997). For a review, see J. J. Joannopoulos *et al.*, *Photonic Crystals* (Princeton Univ. Press, Princeton, NJ, 1995).
3. M. M. Fejer *et al.*, *IEEE J. Quantum Electron.* **QE-28**, 2631 (1992).
4. D. Feng *et al.*, *Appl. Phys. Lett.* **37**, 607 (1980); Y. L. Lu *et al.*, *ibid.* **59**, 516 (1991); Y. L. Lu *et al.*, *ibid.* **68**, 1467 (1996); Y. Q. Lu *et al.*, *ibid.* **69**, 3155 (1996); Y. Lu *et al.*, *Science* **276**, 2004 (1997).
5. L. Ye *et al.*, *Phys. Rev. Lett.* **69**, 3080 (1992).
6. M. S. Kushwaha *et al.*, *ibid.* **71**, 2022 (1993).
7. M. M. Sigalas *et al.*, *Phys. Rev. B* **50**, 3393 (1994); M. S. Kushwaha and P. Halevi, *Appl. Phys. Lett.* **64**, 1085 (1994); J. P. Dowling, *J. Acoust. Soc. Am.* **91**, 2539 (1992); M. M. Sigalas, *ibid.* **101**, 1256 (1997); F. R. Montero de Espinosa *et al.*, *Phys. Rev. Lett.* **80**, 1208 (1998).
8. P. Sheng, Ed., *Scattering and Localization of Classical Waves in Random Media* (World Scientific, Singapore, 1990).
9. S. N. Zhu *et al.*, *Science* **278**, 843 (1997); S. N. Zhu *et al.*, *Phys. Rev. Lett.* **78**, 2752 (1997).
10. K. M. Ho *et al.*, *Phys. Rev. Lett.* **65**, 3152 (1990).
11. J. B. Pendry and A. Mackinnon, *ibid.* **69**, 2772 (1992); H. Dong and S. Xiong, *J. Phys. Condens. Matter* **5**, 8849 (1993); M. M. Sigalas and C. M. Soukoulis, *Phys. Rev. B* **51**, 2780 (1995).
12. J. D. Turner and A. J. Pretlove, *Acoustics for Engineers* (Macmillan, Houndmills, UK, 1991), pp. 27–29; L. Meirovitch, *Elements of Vibration Analysis* (McGraw-Hill, New York, 1975), pp. 281–284.
13. K. Huang, *Proc. R. Soc. London A* **208**, 352 (1951); M. Born and K. Huang, *Dynamical Theory of Crystal Lattices* (Oxford Univ. Press, Oxford, 1954).
14. C. H. Henry and J. J. Hopfield, *Phys. Rev. Lett.* **15**, 964 (1965).
15. $\varepsilon = 84.1$, $\varepsilon_0 = 8.854 \times 10^{-12}$ F/m, $v = 3600$ m/s, $e_{15} = 3.8$ C/m^2, $\rho = 4.64 \times 10^3$ kg/m^3 [Y. Nakagawa *et al.*, *J. Appl. Phys.* **44**, 3969 (1973)].

16. We are grateful to the State Key Program for Basic Research of China, the National Natural Science Foundation Project of China (contract 69708007), and the National Advanced Materials Committee of China for their support of this work.

1 February 1999; accepted 27 April 1999

Middle Eocene Seawater pH and Atmospheric Carbon Dioxide Concentrations

Paul N. Pearson[1]* and Martin R. Palmer[2]

The carbon dioxide content of the atmosphere [measured as the partial pressure of CO_2 (pCO_2)] affects the content of the surface ocean, which in turn affects seawater pH. The boron isotope composition ($\delta^{11}B$) of contemporaneous planktonic foraminifera that calcified their tests at different water depths can be used to reconstruct the pH-depth profile of ancient seawater. Construction of a pH profile for the middle Eocene tropical Pacific Ocean shows that atmospheric pCO_2 was probably similar to modern concentrations or slightly higher.

Earth's climate has cooled markedly in the last 50 million years from a peak of warmth in the early Eocene (*1*). One explanation for this cooling invokes plate tectonic movements and reorganization of ocean currents (*2*). Another is that concentrations of greenhouse gases, especially CO_2, have declined in the atmosphere (*3–5*).

The period of greatest uncertainty in CO_2 concentrations is the middle to late Eocene, which followed an interval of extreme warmth in the early Eocene but preceded dramatic cooling in the earliest Oligocene (*6*). There is much less evidence for widespread hydrothermal, tectonic, and volcanic activity (and hence CO_2 emission) in this interval than in the Cretaceous to early Eocene (*7–10*), and yet world climate was still warm and equable compared with that of the present day (*11*). Some authors have suggested that middle Eocene pCO_2 was two to six times as high as the preindustrial level of 280 ppm (*3, 12–16*), whereas others have suggested values similar to that concentration or only slightly higher (*17–19*). These estimates rely on a variety of relatively indirect methods such as carbon mass balance modeling (*3, 13, 15, 18–19*), interpretation of the $\delta^{13}C$ record in marine sediments (*12, 14*) and paleosols (*17*), or studies of plant leaf morphology (*16*).

The $\delta^{11}B$ of foraminiferal calcite may provide a more direct measure of atmospheric pCO_2 because it reflects the pH of the surface seawater in which the organisms calcified, which is closely dependent on pCO_2 (*20*). By analyzing multiple species that lived at different depths in the ocean, it is possible to reconstruct a pH-depth profile for the upper few hundred meters of the water column (*21*). This allows paleo sea surface pH to be estimated with some confidence, from which pCO_2 can be inferred.

We selected a sample of well-preserved pelagic carbonate from the middle Eocene of the tropical Pacific [Ocean Drilling Program sample 143-865C-6H/2, 65 to 67 cm; lower Biozone P12; dated to approximately 43 million years ago (Ma)]. The sample has a diverse foraminiferal assemblage, which indicates a warm, oligotrophic and well-stratified water column, an inference that is supported by sedimentological and geochemical evidence (*22*). Monospecific splits of 50 to 250 specimens of a variety of species were picked for $\delta^{11}B$ analysis (*21*) (Table 1). Plankton species were assigned to calcification depths (mixed layer, intermediate, thermocline, and deep) on the basis of previous paleobiological research and $\delta^{18}O$ and $\delta^{13}C$ analyses (*22–27*). A single split of benthic foraminifera was also prepared, but because they are scarce in the

[1]Department of Earth Sciences, University of Bristol, Bristol BS8 1RJ, UK. [2]T. H. Huxley School, Royal School of Mines, Imperial College, Prince Consort Road, London SW7 2BP, UK.

*To whom correspondence should be addressed. E-mail: paul.pearson@bristol.ac.uk